Finite Element Analysis of the Dynamic Behaviour of an Engine Block and Comparison with Experimental Modal Test Results

Walter Ott, Hans-Jürgen Kaiser, Jürgen Meyer, Ford-Werke AG, Köln

Abstract

The combustion engine is the main source of noise and vibration in modern vehicles. Today the finite element method (FEM) is the most important CAE tool to assist the engineer in the early stage of the development of an engine structure. The generation of the model is the most time consuming part of the FEM analysis. For reliable predictions a good compromise must be found between modelling effort and necessary accuracy of results. In this paper, two shell-solid element models and two solid element models of a typical 4-cylinder in-line engine block are compared. The natural modes for these four models were calculated up to 2kHz with MSC/NASTRAN SOL 3 and SOL 63 respectively. The analytical results have been compared with modal test data. The assessment of the calculated eigenvectors was based on computer animation of the mode shapes and the evaluation of the MAC (modal assurance criteria) values. The shell-solid models show a good agreement with the measured frequencies, whereas the solid models produce too high frequencies especially for the torsion modes.

1 Introduction

For the successful design of new engines an accurate prediction of noise and vibration behaviour of the engine is required. Currently, empirical and test based methods are widely used for this purpose.

All these methods have the disadvantage that they are only feasible if an engine prototype is available. To achieve a noise reduction the noise is measured, the structure is then modified accordingly, and the cycle is repeated until a satisfactory result is obtained. The main drawbacks of this procedure are loss of time and high costs.

To overcome these problems and to support design decisions in the very early design phase when no prototypes are available, the FEM has become the major tool of the engineer today.

In an engine the main excitation force resulting from oscillating masses and the combustion process are introduced into the cylinder block through the main bearings of the crankshaft. The energy transferred to the engine surfaces results in surface vibrations which leads to

noise radiation of these surfaces. The investigation of 4-cylinder in-line gasoline engines by measuring the radiated sound power from the engine block shows that about 70-90 % of the entire sound power is radiated in the frequency range up to 2 kHz [1, 2]. This means for a suitable FEM-based prediction of the engine noise radiation the finite element model of the engine block should be able to describe the dynamic behaviour of this component up to a frequency of 2 kHz.

For the finite element modelling of engine blocks beam, shell and solid elements are usually used. Elements with linear shape functions have been found most useful in engineering practice. This paper deals with two different types of finite element models for engine vibration calculation.

- Solid models:

  With a sufficient number of elements, these models should represent the actual engine block the most accurately. The necessary number of elements may be very high, especially for elements with linear shape functions because more than one layer of elements over the thickness may be required for bending representation.
  With the same mesh density in membrane direction as a shell model a solid model has in general a higher number of degrees of freedom. This results in a higher computing time and a higher amount of result data for the postprocessing. Also, the modelling and remodelling of variants may become very time consuming. The solid model of a 4-cylinder in-line engine block is shown in fig. 1.

- Shell and solid models:

  In these models shell elements are used to model the main part of the engine block. Thicker parts such as bearings and massive ribs are modelled with solid elements. The connections of shell to solids are done by overlapping the shell elements with the solid region. The major advantage of a shell-solid model is that the finite element model generation is not as time consuming as for a pure solid model. Moreover model modifications are a lot easier to realize. Fig. 2 shows a typical shell-solid model of an engine block.

As already mentioned the accuracy of a FEM calculation is basically dependent on the finite element representation of the considered structure. On the other hand the finite element mesh generation for a complex structure takes about 80 % of the total effort of a FEM analysis [3, 4].

At Ford, investigations were carried out to give evidence how to generate an optimal finite element model of an engine block for the described purpose, considering the numerical accuracy and the effort for model generation [4, 5].

2 Finite element models

In the investigations [4, 5] mentioned above, three different finite element models of an 4-cylinder in-line engine block were compared for a frequency range up to 2 kHz. The finite element models are shown in fig. 3-5. Model 1 and 2 are combined shell-solid models and model 3 is a pure solid model (elements with linear shape functions were used exclusively). Model 4 is almost identical with model 3, but uses solid elements with quadratic shape functions for improved accuracy instead of the elements with linear shape functions of model 3 shown in fig. 5.

The grid and element distribution of the four models is shown in table 1.

	Model 1	Model 2	Model 3	Model 4
GRID	4040	7096	9166	32241
TRIA3	102	115	-	-
QUAD4	2328	4156	-	-
PENTA6	67	59	137	-
HEXA8	995	1439	4698	-
PENTA15	-	-	-	133
HEXA20	-	-	-	4692

Table 1 Grid- and element numbers in the FE-models

3 Finite element analysis

The natural modes for the four models were calculated under free-free conditions on a CRAY-XMP computer using MSC/NASTRAN. For models 1-3 SOL 3 with GDR (Generalized Dynamic Reduction) and MGIV (Modified Givens Method) was used.
The natural modes for model 4 were calculated on a CRAY-YMP computer with the superelement solution SOL 63 using the Lanczos method for each superelement.
Therefore, the engine block model 4 was divided into 9 superelements according to fig. 6.
The superelement tree of this configuration is shown in fig. 7.

The material data of a mild steel were used in the analysis with:

Young's Modulus: $E = 210{,}000\ N/mm^2$

Poison's Ratio: $\nu = 0.3$

Mass Density: $\rho = 7{,}850\ kg/m^3$

The tables 2-5 summarize the results of the normal modes calculations. The association of the eigenmodes to a subjective mode description is based on computer-animation of the eigenvectors.

No.	Freq. [Hz]	Mode
1	742	1. torsion
2	1236	1. lat. bending
3	1539	front bearing
4	1579	bearing
5	1592	2. torsion
6	1598	bearing
7	1621	bearing
8	1814	all bear. in phase

Table 2 Natural frequencies model 1

No.	Freq. [Hz]	Mode
1	706	1. torsion
2	1220	1. lat. bending
3	1435	2. torsion
4	1546	front bearing
5	1557	bearing
6	1574	bearing
7	1598	bearing
8	1790	all bear. in phase

Table 3 Natural frequencies model 2

No.	Freq. [Hz]	Mode
1	866	1. torsion
2	1393	1. lat. bending
3	1671	bearing
4	1676	front bearing
5	1703	bearing
6	1738	bearing
7	1872	2. torsion
8	1942	all bear. in phase

Table 4 Natural frequencies model 3

No.	Freq. [Hz]	Mode
1	827	1. torsion
2	1344	1. lat. bending
3	1577	bearing
4	1592	bearing
5	1610	front bearing
6	1650	bearing
7	1837	2. tors. + bearing
8	1855	all bear. in phase

Table 5 Natural frequencies model 4

Table 6 shows the CPU-time used for the four analysis runs with the different models.

	Model 1	Model 2	Model 3	Model 4
CPU [sec]	988	3358	2143	25850

Table 6 CPU-time of the NASTRAN runs

For the CPU-time comparison the CPU-time for model 4 should be multiplied by a factor of about 2. This is the average CPU-time ratio between the CRAY-XMP and YMP for MSC/NASTRAN runs. Comparing the CPU-times, it becomes evident that the calculation time for the model 4 would not be acceptable for a design optimization procedure in the early design stage of an engine.

4 Experimental modal analysis

For the verification of the analytical results, an experimental modal analysis with the engine block was accomplished [5]. Similar comparisons which can be found in the literature are mostly based on original cast iron engine blocks [6-9]. Geometry data of cast iron engine blocks, like wall thickness, may differ up to 50 % from specification [6, 7]. To avoid geometric inaccuracies of the test model, a welded mild steel construction of the engine block was built (fig. 8). Compared to a cast engine block this construction has the advantage that the geometric deviation of the finite element model geometry is very low.
Also the used mild steel is a very homogeneous material with well defined material data.
The mass comparison of the four FE-models with the test model gives a mass difference of less than 3 % for all models. After the welding procedure the engine block was stress-relieved by annealing. A frequency analysis carried out before and after the annealing shows no influence of this procedure
At Ford the LMS (Leuven Measurement System)-system CADA-X has proved efficient for experimental modal analysis. As in a finite element analysis, the considered structure is divided into a number of nodes which represent the structure. The modal representation of the engine block is shown in fig. 9.
The engine block was excited with an impulse hammer in node 38 in x-direction. The accelerations were measured with three-axial accelerometers. Fig. 10 represents the summarized measured transfer functions of all degrees of freedom. The natural frequencies of the structure can be found at the maximum values of this transfer function. For the identification of eigenmodes which are close together in the frequency range special curvefit algorithms are used in the LMS-software. Table 7 shows the results of the experimental modal analysis.

No.	Freq. [Hz]	Mode
1	745	1. torsion
2	1274	1. lat. bending
3	1497	2. torsion
4	1570	front bearing
5	1583	bearing
6	1779	bearing
7	1800	all bear. in phase
8	1814	bearing

Table 7 Natural frequencies modal test

The association of the eigenmodes to a subjective mode description is based on computer-animation of the mode shapes by the LMS-system.

5 Result comparison

For the four finite element analysis results (table 2-5) and the modal test results (table 7) eight eigenmodes were found in the frequency range up to 2 kHz for each result data set. Comparison of the obtained mode shapes leads to a subdivision into:

- Three global torsional and bending modes
- Five local bearing modes

From these eight eigenmodes five can be found in all five data sets. These are the three global modes and two bearing modes. The shapes of these five characteristic eigenmodes are shown in fig. 11-15 for model 2 respectively.

The finite element results for these five eigenmodes related to the test results are shown in fig. 16. Model 1 and 2 show a very good agreement with the measured frequencies. That too low frequencies are achieved especially for the three global modes could be caused by a too flexible representation of corners by shell elements [10]. With the introduction of constraints (MPC's, RBE's) in these areas an improvement of the model behaviour may be possible, but is unusual in engineering practice due to the high modelling expenditure.

The highest deviation in frequency was found for the model 3. Although this HEXA8-model represents the engine block highly accurately from an optical point of view (fig. 5), it is far to stiff. One reason for this could be the bad bending behaviour of these elements.

In addition to the subjective comparison of eigenmodes described above an objective correlation of the calculated and measured mode shapes was carried out based on the Modal Assurance Criterion (MAC). The definition of the MAC-value is given by the following expression.

$$MAC = \frac{\left| \sum_{j=1}^{m} \Phi_{1(j)}^{*} \quad \Phi_{2(j)} \right|^{2}}{\left(\sum_{j=1}^{m} \Phi_{1(j)}^{*} \quad \Phi_{1(j)} \right) \quad \left(\sum_{j=1}^{m} \Phi_{2(j)}^{*} \quad \Phi_{2(j)} \right)}$$

In this formula, Φ is the eigenvector, Φ^{*} its conjugate complex form and m the number of degrees of freedom (DOF). The MAC-value for two eigenvectors Φ_1 and Φ_2 can range from 0 to 1. A large value indicates a good correlation between the considered modes. If the eigenvectors Φ_1 and Φ_2 have different number of DOF's the larger eigenvector is reduced to achieve an identical number of DOF's for both eigenvectors.

In a first step, the results from the finite element analysis were compared with each other. Table 8-13 show the calculated MAC-value matrices. The model which is first mentioned in the table title is related to the horizontal axis of the table.

8	0	0	0	0	0	0	0	0.98
7	0	0	0	0	0	0	0.97	0
6	0	0	0	0	0.48	0.88	0	0
5	0	0	0	0.98	0	0	0	0
4	0	0	0.90	0	0.12	0	0	0
3	0	0	0	0	0.39	0	0	0
2	0	0.99	0	0	0	0	0	0
1	0.99	0	0	0	0	0	0	0
	1	2	3	4	5	6	7	8

Table 8 MAC-matrix: Model 1 - Model 2

8	0	0	0	0	0	0	0	0.97
7	0	0	0	0	0.35	0	0	0
6	0	0	0	0	0	0	0.97	0
5	0	0	0	0	0.48	0.84	0	0
4	0	0	0	0.93	0	0	0	0
3	0	0	0.79	0	0.15	0	0	0
2	0	0.97	0	0	0	0	0	0
1	0.98	0	0	0	0	0	0	0
	1	2	3	4	5	6	7	8

Table 9 MAC-matrix: Model 1 - Model 3

8	0	0	0	0	0	0	0.44	0.89
7	0	0	0	0	0	0.91	0	0
6	0	0	0	0.46	0.48	0	0	0
5	0	0	0	0.37	0.21	0	0.19	0
4	0	0	0.83	0.12	0	0	0	0
3	0	0	0.12	0.30	0.44	0	0	0
2	0	0.97	0	0	0	0	0	0
1	0.98	0	0	0	0	0	0	0
	1	2	3	4	5	6	7	8

Table 10 MAC-matrix: Model 1 - Model 4

8	0	0	0	0	0	0	0	0.99
7	0	0	0.91	0	0	0	0	0
6	0	0	0	0	0	0	0.98	0
5	0	0	0	0	0	0.98	0	0
4	0	0	0	0	0.97	0	0	0
3	0	0	0	0.96	0	0	0	0
2	0	0.98	0	0	0	0	0	0
1	0.99	0	0	0	0	0	0	0
	1	2	3	4	5	6	7	8

Table 11 MAC-matrix: Model 2 - Model 3

8	0	0	0	0	0	0	0.45	0.92
7	0	0	0	0	0	0.92	0	0
6	0	0	0	0.39	0.66	0	0	0
5	0	0	0.80	0.15	0	0	0	0
4	0	0	0.22	0.47	0.21	0	0	0
3	0	0	0	0	0	0	0.48	0
2	0	0.98	0	0	0	0	0	0
1	0.99	0	0	0	0	0	0	0
	1	2	3	4	5	6	7	8

Table 12 MAC-matrix: Model 2 - Model 4

8	0	0	0	0	0	0	0.42	0.95
7	0	0	0	0	0	0	0.64	0
6	0	0	0	0	0	0.97	0	0
5	0	0	0	0	0.77	0	0	0
4	0	0	0.68	0.28	0	0	0	0
3	0	0	0.39	0.42	0.12	0	0	0
2	0	1.0	0	0	0	0	0	0
1	1.0	0	0	0	0	0	0	0
	1	2	3	4	5	6	7	8

Table 13 MAC-matrix: Model 3 - Model 4

For the models 1-3 a high correlation of the eigenmodes is found. Why the MAC-values calculated for model 4 show a somewhat worse correlation is not clear to the authors. Surprising is the very good correlation of model 2 and 3 although the calculated natural frequencies differ considerably for these two models.

In table 14 the modal test results are compared with themselves.

8	0	0	0	0	0	0	0.23	1.0
7	0	0	0	0	0	0.31	1.0	0.23
6	0	0	0.13	0	0.13	1.0	0.31	0
5	0	0	0	0.29	1.0	0.13	0	0
4	0	0	0	1.0	0.29	0	0	0
3	0	0	1.0	0	0	0.13	0	0
2	0	1.0	0	0	0	0	0	0
1	1.0	0	0	0	0	0	0	0
	1	2	3	4	5	6	7	8

Table 14 MAC-matrix: Test - Test

The MAC-matrix shows a coupling between modes 4 and 5, modes 6 and 7, and modes 7 and 8. The calculated MAC-values for these modes are quite low, and because modes 4 and 8 are bearing modes it is highly probable that the modes are independent.

In the next step, the analytical results were compared with the modal test data. The calculation of the MAC-matrices for all FE-models results in a very bad correlation with the test data. Only after splitting the engine block into a block component and a bearing component according to fig. 9 was the association of the mode shapes found by the computer-animation confirmed.

The calculated MAC-values for all four FE-models are similar. Representative for these results the MAC-matrix for the block and bearing component of model 2 is given in table 15.

8	0	0	0	0	0	0	0.28	0.26
7	0	0	0	0	0	0	0	0
6	0	0	0	0	0.16	0	0	0
5	0	0	0	0	0.26	0	0	0
4	0	0	0	0	0.63	0	0	0
3	0	0	0.46	0	0	0.16	0	0
2	0	0.61	0	0	0	0	0	0
1	0.83	0	0	0	0	0	0	0
	1	2	3	4	5	6	7	8

Table 15 MAC-matrix Model 2 - Test block component

8	0	0	0.15	0	0	0.30	0.42	0.36
7	0	0	0.12	0	0	0	0	0
6	0	0	0	0	0.35	0	0	0
5	0	0	0	0	0	0	0	0
4	0	0	0.11	0.49	0.12	0	0	0
3	0	0	0.14	0	0	0	0	0
2	0	0.90	0	0	0	0	0	0
1	0.92	0	0	0	0	0	0	0
	1	2	3	4	5	6	7	8

Table 16 MAC-matrix Model 2 - Test bearing component

The values show a fair correlation but the interpretation of these results is still difficult. The reason for this could be that with the distribution of measuring points over the engine block surfaces a weighting of specific structure parts occur. Because only a low number of points

are measured (58 in the performed modal test) this can result in poorly defined MAC-values [11]. The use of MAC-values requires some experience in that method to avoid drawing the wrong conclusions.

6 Conclusion

The calculation of the natural modes of a 4-cylinder in-line engine block with four different FE-models shows that model 1, a combined shell-solid model with a moderate mesh density, and model 2, a combined shell-solid model as model 1 but with higher mesh density, can be used to describe the dynamic behaviour up to a frequency of 2 kHz with sufficient accuracy. Five eigenmodes which are present in all five data sets have been determined by computer-animation of the eigenvectors. The comparison of the natural frequencies from the finite element analysis with data derived from modal tests for these five eigenmodes shows a good agreement for model 1 and 2. It came out that model 3, a solid model based on elements with linear shape functions, is too stiff to represent the considered engine block with sufficient accuracy. Model 4, a solid model based on elements with quadratic shape functions, agrees good for the bearing and the bending modes but results in too high frequencies for the two torsion modes.
Only fair correlation have been found for the eigenmode assessment between analytical data and test data based on the MAC criterion.
An important result of the present investigation is that a solid model representation of the engine block is not necessary in the frequency range up to 2 kHz.

7 References

[1] Brüdgam, W.: Reduzierung des Motorgeräusches anhand strukturmechanischer Analysen. VDI-Berichte, Nr. 499 (1983), p. 133-139.

[2] Maekawa, K., Morita, S.: Calculation of Radiated Noise from Cylinder Block Using Finite Element Model. Int. J. of Vehicle Design, Vol. 6 (1985), No. 2, p. 228-239.

[3] Knoll, G.: Kostensparende Strukturanalyse nach der finite Elemente Methode mit Hilfe rationeller Modellaufbereitung. Konstruktion, Nr. 31 (1979).

[4] Heuer, P.: Vergleichende Untersuchung der Zuverlässigkeit von FEM-Ergebnissen bei Einsatz von Schalen- bzw. Volumenelementen für den Motorblock eines Vierzylinderreihenmotors. Fachhochschule Köln, Köln, Jan. 1989.

[5] Fischerkeller, R.: Vergleichende Untersuchung der mit der FEM berechneten Eigenformen und Eigenfrequenzen für den Motorblock eines 4-Zylinder-Reihenmotors mit gemessenen Werten. Fachhochschule Köln, Köln, Sep. 1989.

[6] Birth, M., Papez, S.: Idealization, Measurement and Calculation of an Engine Block. SAE-Paper 820438, 1982.

[7] Tyrell, R.J., Croker, D.M.: Engine Noise: Practicalities and Prediction, Part 2 - Finite Element Analysis. SAE-Paper 870978, 1987.

[8] Schulze-Schwering, W.: Einsatz von Strukturanalyse-Methoden bei der Konstruktion von geräuscharmen Verbrennungsmotoren. VDI-Berichte, Nr. 444 (1982), p. 51-58.

[9] Brandeis, J.P.: The Use of Finite Element Techniques to Predict Engine Vibration. SAE-Paper 820436, 1982.

[10] Chargin, M.: Advanced Modeling and Solution Topics in MSC/NASTRAN. MacNeal-Schwendler GmbH, München, 1988.

[11] Ellenbroek, M.H.M., Wijker, J.J., de Boer, A.: Influence of Reduction and Interpolation Methods on the Correlation of Calculated and Measured Data of a Solar Array. Proceedings of the 14th International Seminar on Numerical Methods in Structural Dynamics. Katholieke Universiteit Leuven, Leuven, 11.-15. Sep. 1989.

8 Figures

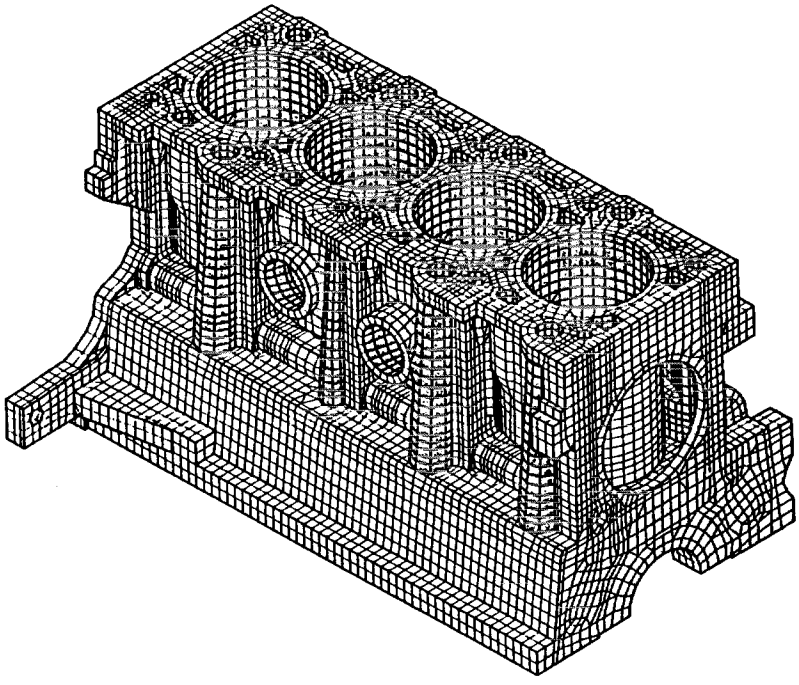

Fig. 1 Solid model of an 4-cylinder in-line engine block

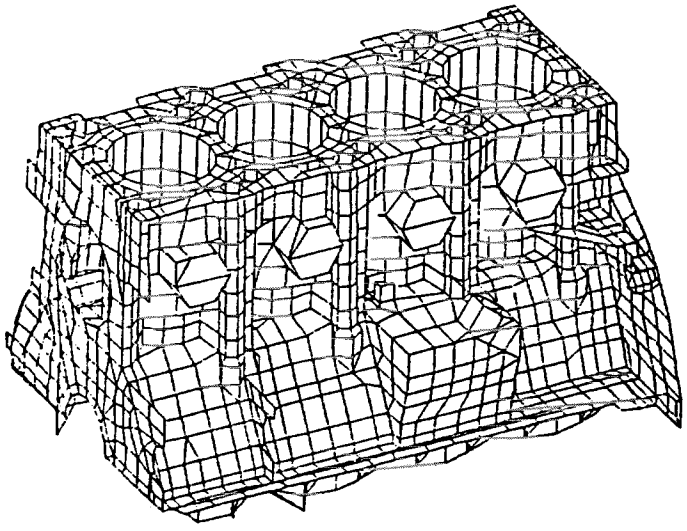

Fig. 2 Shell-solid model of an 4-cylinder in-line engine block

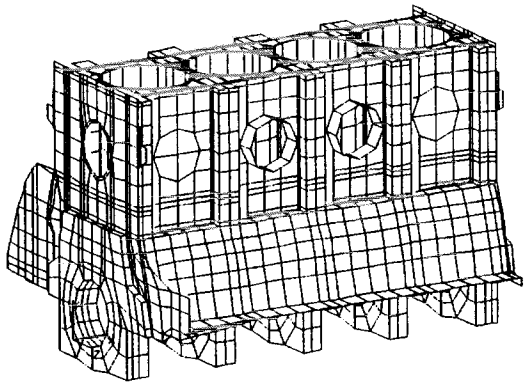

Fig. 3 Model 1 (course shell-solid)

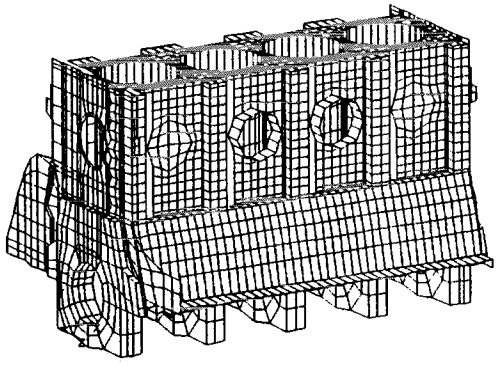

Fig. 4 Model 2 (fine shell-solid)

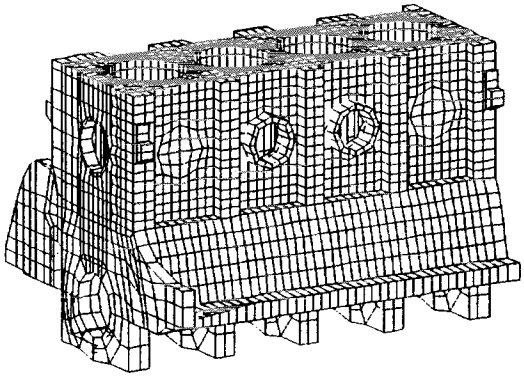

Fig. 5 Model 3 (solid)

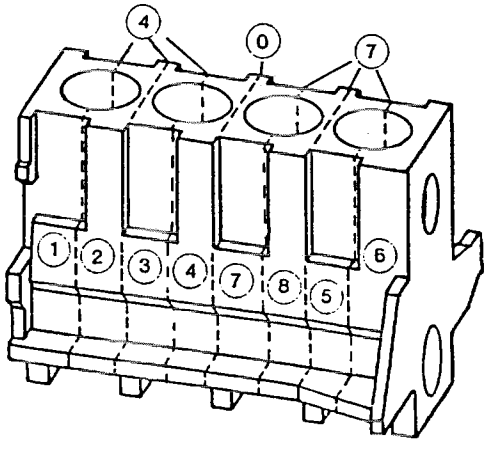

Fig. 6 Model 4: Superelement division

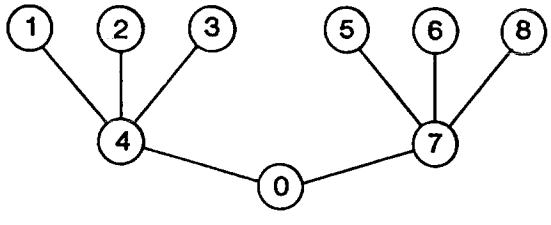

Fig. 7 Model 4: Superelement tree

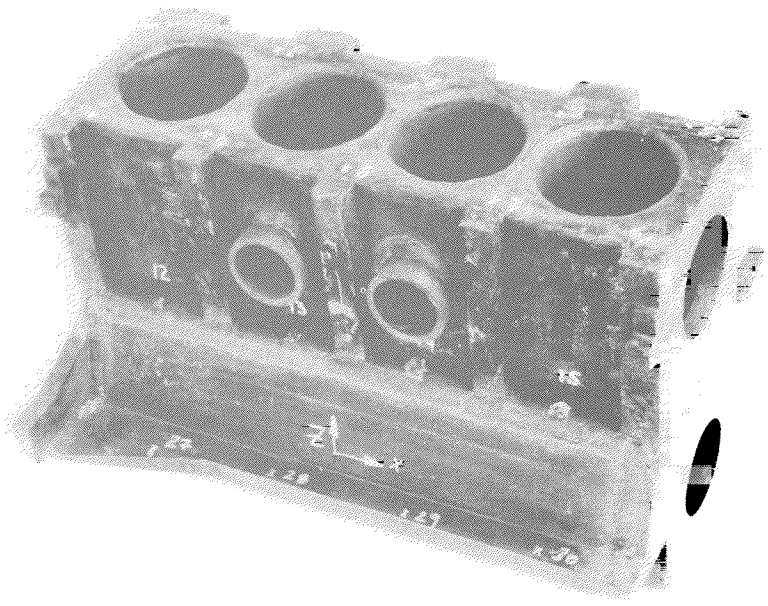

Fig. 8 Test model

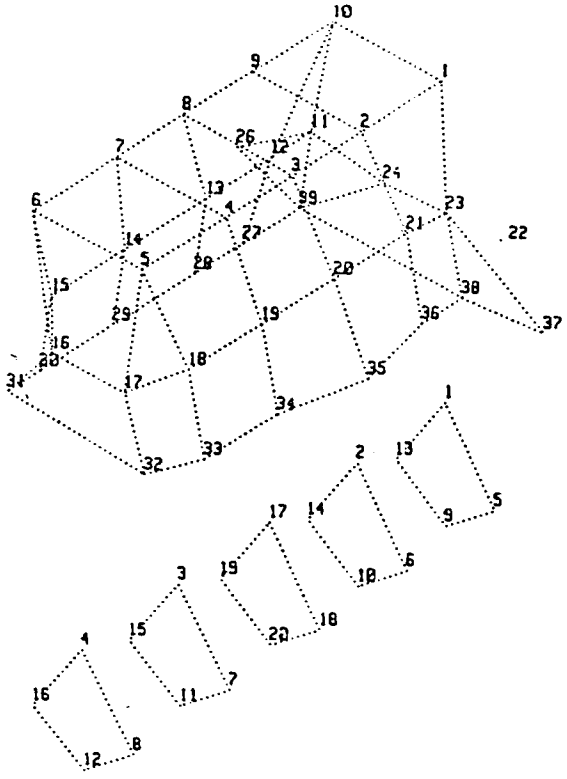

Fig. 9 Mesh for modal testing

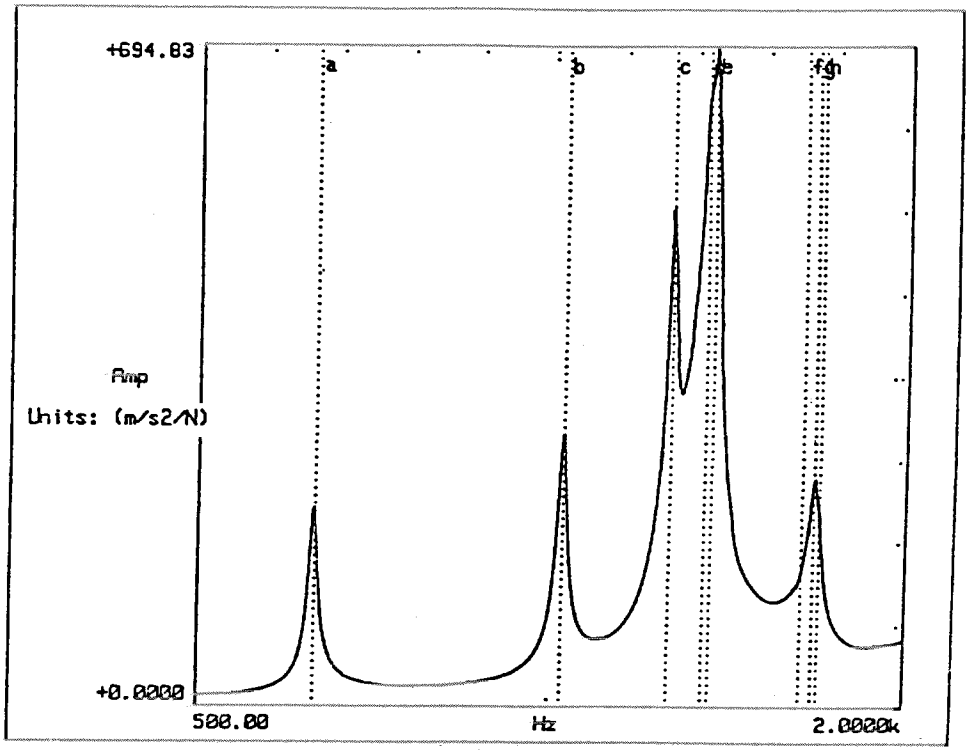

Fig. 10 Summarized measured transfer functions

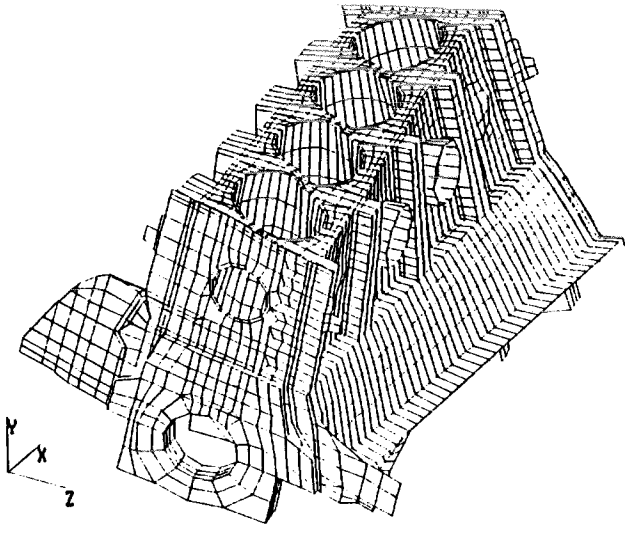

Fig. 11 Model 2: 1. Torsion mode

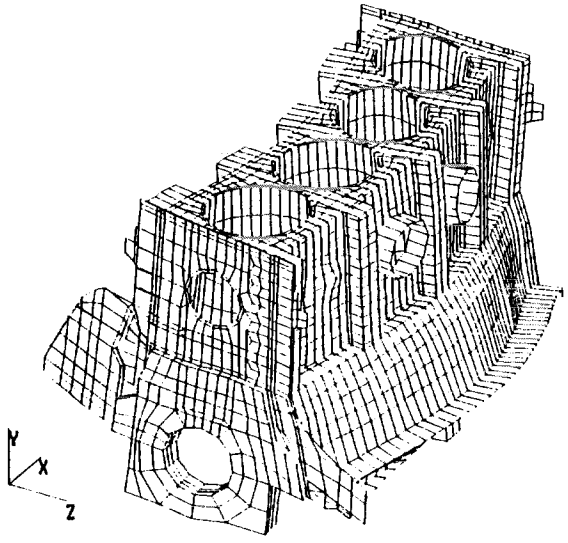

Fig. 12 Model 2: 1. Bending mode

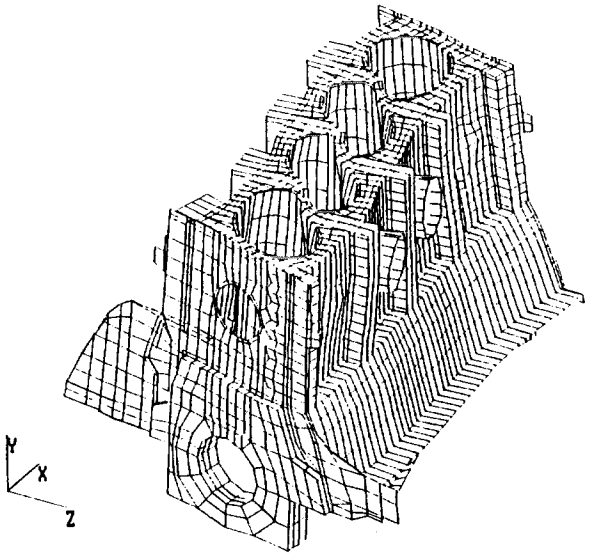

Fig. 13 Model 2: 2. Torsion mode

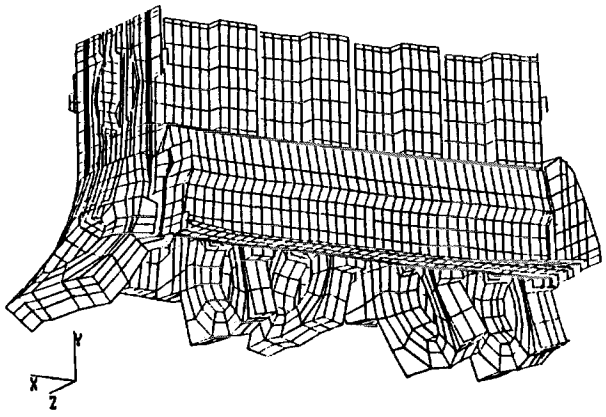

Fig. 14 Model 2: Front bearing mode

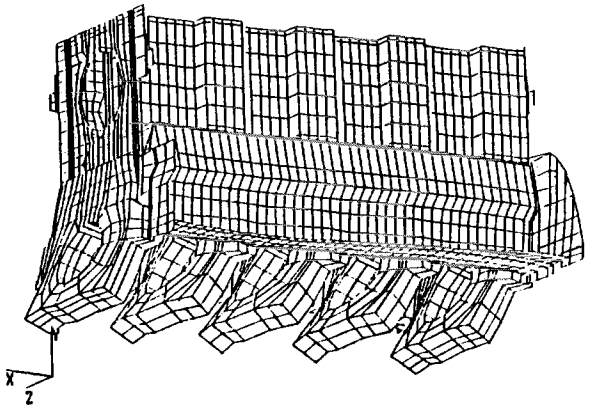

Fig. 15 Model 2: All bearings in phase mode

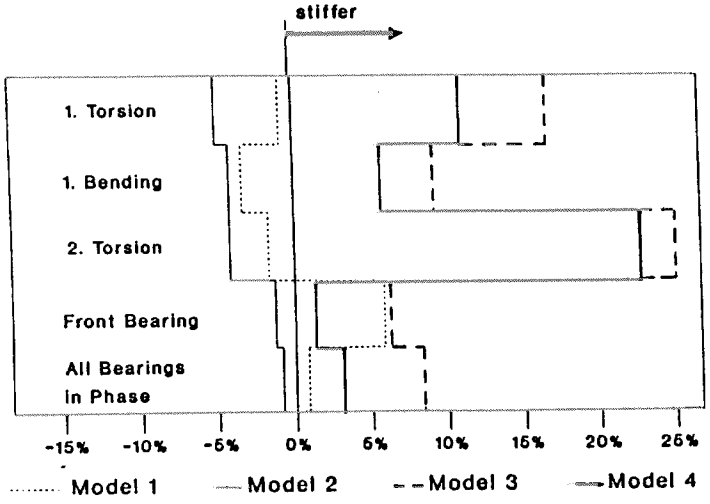

Fig. 16 Calculated frequencies related to the test results